

Weyl superconductors

Tobias Meng¹ and Leon Balents²

¹*Institut für Theoretische Physik, Universität zu Köln, Zùlpicher Str. 77, 50937 Köln, Germany*

²*Kavli Institute for Theoretical Physics, University of California, Santa Barbara, CA 93106, USA*

(Dated: October 22, 2018)

We study the physics of the superconducting variant of Weyl semimetals, which may be realized in multilayer structures comprising topological insulators and superconductors. We show how superconductivity splits each Weyl node into two. The resulting Bogoliubov Weyl nodes can be pairwise independently controlled, allowing to access a set of phases characterized by different numbers of bulk Bogoliubov Weyl nodes and chiral Majorana surface modes. We analyze the physics of vortices in such systems, which trap zero energy Majorana modes only under certain conditions. We finally comment on possible experimental probes, thereby also exploiting the similarities between Weyl superconductors and 2-dimensional $p + ip$ superconductors.

PACS numbers:

I. INTRODUCTION

The discovery of topological insulators has stimulated a broad inquiry into topological features of electronic energy bands. Such features are present not only in fully gapped systems but also in gapless ones. Of particular recent interest are semimetals (zero gap semiconductors) with Fermi points, where conduction and valence bands touch at isolated momenta in the Brillouin zone. In three dimensions, a linear touching between two non-degenerate bands is a Weyl point,¹⁻³ and is completely robust to all perturbations which do not break translational symmetry. Such Weyl nodes are predicted to lead to a variety of measurable consequences, including unusual surface states whose Fermi surface is open (“Fermi arcs”), unusual Hall effects, and other unusual transport features, and have been studied in a number of systems.³⁻¹⁷ Generically, Weyl points require a system with strong spin-orbit coupling, and in addition the condition that the bands be non-degenerate requires that at least either inversion or time-reversal symmetry be broken.^{9,18} This might occur in a bulk material through magnetic order or a non-centrosymmetric crystal structure, but Weyl points can also be engineered. In particular, an appropriate superlattice of alternating normal and topological insulators has been shown to display Weyl points.^{5,19}

Weyl fermions have been discussed extensively in the context of the A phase of ³He, which also exhibits Weyl quasiparticles. ³He also supports the B phase, in which quasiparticles are fully gapped, but which nevertheless possesses interesting topological properties.² In this paper, we explore the connection of Weyl semimetals to Weyl and topological superconductors, and more generally the effects of superconductivity on Weyl semimetals. Specifically we consider another class of engineered structures, in which the normal insulator of the aforementioned superlattice is replaced by a (conventional, s-wave) superconductor. Simple arguments show that only the Weyl semimetal produced by time-reversal symmetry breaking, and not the one produced by non-

centrosymmetry, leads to non-trivial superconducting states. Focusing on the former, we find that a variety of superconducting phases, with and without Weyl points, and with varying topological features, can be tuned, depending upon the degree of time-reversal symmetry breaking and the magnitude of the superconducting proximity effect upon the topological insulating layers of the superlattice.

Each of these phases may be characterized in a number of ways, which we discuss in the main text. In the bulk, they may be parametrized by the number, location, and chirality of Weyl points. At surfaces, depending upon both the phase and the surface orientation, one or several branches of chiral Majorana states may be present, and extend over a varying range of momenta in the surface Brillouin zone. Gapless Majorana states may also be present at vortex cores, again depending in detail upon vortex orientation and phase. These Majorana modes are relatives of those proposed for use in quantum computing in two dimensional topological superconductors.

The paper is organized as follows. In Sec. II, we discuss how Weyl superconductors can be engineered in superlattices of superconductors and topological insulators, and derive the corresponding model. Sec. III is then devoted to the characterization of this Hamiltonian. We analyze how superconductivity acts on Weyl electrons in the bulk and discuss the related topological surface physics. Based thereon, a topological phase diagram is constructed. In Sec. IV, we analyze the physics of vortices, which under certain conditions can bind Majorana zero modes. We close with some proposals for experimental signatures based on thermal and electrical transport, which are given in Sec. V.

II. SUPERLATTICE

A Weyl semimetal can be understood as an intermediate phase between a normal insulator (NI) and a topological insulator (TI), arising due to a perturbation of the transition between the two.¹⁸ One pathway to engineer

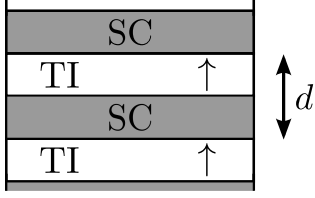


FIG. 1: The proposed heterostructure for an experimental realization of Weyl superconductors. Magnetically doped layers of a topological insulator (TI) are alternated with layers of an s-wave superconductor (SC). The period of the superlattice is d . The arrows in the TI layers depict their magnetization, which is along the superlattice axis.

Weyl semimetals is thus the stacking of layers of topological and normal insulators.⁵ In the very same spirit, a Weyl superconductor arises upon alternating thin layers of topological insulators and standard s-wave BCS superconductors (SC). In such a structure, sketched in Fig. 1, the proximity effect induces superconductivity in the surface states of the TI layers.

As remarked in the Introduction, to realize a Weyl semimetal requires breaking of either time reversal or inversion symmetry. In the bulk of this paper we focus on the time reversal symmetry breaking case, as it leads to much more non-trivial results in the presence of superconductivity. Indeed, in Appendix A, we show that when inversion symmetry is instead broken, while time reversal is preserved, superconducting proximity effect leads directly to a gapped, trivial phase. Specifically we model the topological insulator layers by a single Dirac node per surface, with an imposed Zeeman splitting which may be considered to arise from an exchange coupling to randomly distributed magnetic impurities ferromagnetically polarized perpendicular to the TI layers, while the coupling between the TI surface modes and the magnetic field of the impurities is neglected as usual in such systems.^{20–24} We assume the individual layers to be thin, such that sample is globally phase coherent. Furthermore, neighboring surface layers are tunnel coupled. Longer range tunneling is assumed to be negligible.

A. Model Hamiltonian

Working in units of $\hbar = 1$, we model the system by the Hamiltonian

$$H = \sum_{\vec{k}_\perp, i, j} c_{\vec{k}_\perp i}^\dagger \mathcal{H}_{ij} c_{\vec{k}_\perp j} + H_{SC}, \quad (1)$$

$$\mathcal{H}_{ij} = v_F \tau^z (\hat{z} \times \vec{\sigma}) \cdot \vec{k}_\perp \delta_{i,j} + m \sigma^z \delta_{i,j} + t_S \tau^x \delta_{i,j} + \frac{1}{2} t_D \tau^+ \delta_{i,j+1} + \frac{1}{2} t_D \tau^- \delta_{i,j-1} \quad (2)$$

$$H_{SC} = \sum_{\vec{k}_\perp, i} \Delta \left(c_{\vec{k}_\perp \uparrow i}^{\text{top} \dagger} c_{-\vec{k}_\perp \downarrow i}^{\text{top} \dagger} + c_{\vec{k}_\perp \uparrow i}^{\text{bot} \dagger} c_{-\vec{k}_\perp \downarrow i}^{\text{bot} \dagger} \right) + \text{h.c.}, \quad (3)$$

where $c_{\vec{k}_\perp i} = (c_{\vec{k}_\perp \uparrow i}^{\text{top}}, c_{\vec{k}_\perp \downarrow i}^{\text{top}}, c_{\vec{k}_\perp \uparrow i}^{\text{bot}}, c_{\vec{k}_\perp \downarrow i}^{\text{bot}})^T$ comprises annihilation operators for electrons of spin up and down in the top and bottom surfaces of layer i with in-plane momentum \vec{k}_\perp . The unit vector along the perpendicular axis is \hat{z} . The Fermi velocity of the Dirac nodes is v_F , for simplicity considered to be the same on each surface, and Pauli matrices $\vec{\sigma}$ act on the real spin. The additional pseudo spin for the top/bottom surface degree of freedom denoted by the Pauli matrices $\vec{\tau}$. The Zeeman mass (half the Zeeman splitting) is m , the tunneling between top and bottom surface of the same TI layer is denoted by t_S , and the tunneling between different TI layers is t_D . The proximity induced superconductivity is characterized by $\Delta = |\Delta|e^{i\varphi}$, with φ being the globally coherent superconducting phase.

We proceed by Fourier transforming the Hamiltonian along \hat{z} , where the superlattice constant is d . After a canonical transformation

$$\sigma^\pm \rightarrow \tau^z \sigma^\pm, \quad \tau^\pm \rightarrow \sigma^z \tau^\pm, \quad (4)$$

and subsequent diagonalization in the $\vec{\tau}$ subspace, the Hamiltonian reads

$$H = \sum_{\vec{k}, l=\pm} c_{\vec{k}l}^\dagger \mathcal{H}_l c_{\vec{k}l} + \sum_{l=\pm} H_{SC,l}, \quad (5)$$

$$\mathcal{H}_\pm = v_F (\hat{z} \times \vec{\sigma}) \cdot \vec{k} + M_\pm(k_z) \sigma^z, \quad (6)$$

$$M_\pm(k_z) = m \pm \sqrt{t_S^2 + t_D^2 + 2 t_S t_D \cos(k_z d)}, \quad (7)$$

$$H_{SC,\pm} = \sum_{\vec{k}} \Delta c_{\vec{k}\uparrow\pm}^\dagger c_{-\vec{k}\downarrow\pm}^\dagger + \text{h.c.}, \quad (8)$$

where $c_{\vec{k}\pm} = (c_{\vec{k}\uparrow\pm}, c_{\vec{k}\downarrow\pm})^T$ is now composed of the appropriate eigenoperators resulting from the diagonalization in the $\vec{\tau}$ -subspace, and \vec{k} being the 3-dimensional momentum. Because the proximity induced superconductivity does not mix the two $\vec{\tau}$ sectors, we can analyze the corresponding subspaces separately.

B. Normal state

A Weyl node corresponds to the vanishing of an eigenenergy of (5) for one momentum. In the case without superconductivity analyzed in Ref. 5, and assuming without loss of generality that $m > 0$ and $t_S/t_D > 0$, two Weyl nodes of opposite chirality can appear in the spectrum of \mathcal{H}_- . They are located at $\vec{k} = (0, 0, \pi/d \pm k_0)^T$ with

$$k_0 = \frac{1}{d} \arccos \left(1 - \frac{m^2 - (t_S - t_D)^2}{2 t_S t_D} \right), \quad (9)$$

as long as the condition

$$m_{c1}^2 = (t_S - t_D)^2 < m^2 < (t_S + t_D)^2 = m_{c2}^2 \quad (10)$$

is fulfilled. For $m^2 < (t_S - t_D)^2$, \mathcal{H}_- describes a trivial insulator, while $m^2 > (t_S + t_D)^2$ corresponds to a quantum anomalous Hall insulator. The Hamiltonian \mathcal{H}_+ , on the other hand, always describes a trivial insulator. It is adiabatically connected to the case $m = 0$ that is topologically trivial.

C. Superconducting state

For the superconducting case, we keep $m > 0$ and $t_S/t_D > 0$, although a different choice does not change our results qualitatively. We start by analyzing the subspace corresponding to $\tau^z = -1$, which in the normal case potentially exhibits Weyl nodes. Technically, superconductivity is taken into account by introducing a particle-hole pseudospin on which the Pauli matrices $\vec{\kappa}$ act, as well as the corresponding Nambu spinors. Using $\psi_{\vec{k}} = (c_{\vec{k}\uparrow-}, c_{\vec{k}\downarrow-}, c_{-\vec{k}\downarrow-}^\dagger, c_{-\vec{k}\uparrow-}^\dagger)^T$, the $\tau^z = -1$ sector of the Hamiltonian can be recast into the form

$$H_- = \frac{1}{2} \sum_{\vec{k}} \psi_{\vec{k}}^\dagger \left[\left(v_F (\hat{z} \times \vec{\sigma}) \cdot \vec{k} + M_-(k_z) \sigma^z \right) \mathbb{1}_{\vec{k}} \right. \\ \left. + \sigma^z \frac{1}{2} (\Delta \kappa^+ + \Delta^* \kappa^-) \right] \psi_{\vec{k}}. \quad (11)$$

Diagonalization of the \vec{k} subspace yields

$$H_- = \frac{1}{2} \sum_{\vec{k}, n=\pm} \Phi_{\vec{k}, n}^\dagger \mathcal{H}_-^{n\Delta} \Phi_{\vec{k}, n}, \quad (12)$$

where

$$\mathcal{H}_-^{\pm\Delta} = v_F (\hat{z} \times \vec{\sigma}) \cdot \vec{k} + M_-^{\pm\Delta}(k_z) \sigma^z, \quad (13)$$

$$M_-^{\pm\Delta}(k_z) = (m \pm |\Delta|) - \sqrt{t_S^2 + t_D^2 + 2t_S t_D \cos(k_z d)}, \quad (14)$$

and

$$\Phi_{\vec{k}, +} = \begin{pmatrix} d_{\vec{k}} \\ d_{-\vec{k}}^\dagger \end{pmatrix}^T, \quad \Phi_{\vec{k}, -} = \begin{pmatrix} f_{\vec{k}} \\ f_{-\vec{k}}^\dagger \end{pmatrix}^T, \quad (15a)$$

$$d_{\vec{k}} = \frac{1}{\sqrt{2}} \left(e^{-i\varphi/2} c_{\vec{k}\uparrow-} + e^{+i\varphi/2} c_{-\vec{k}\downarrow-}^\dagger \right), \quad (15b)$$

$$f_{\vec{k}} = \frac{1}{\sqrt{2}i} \left(e^{-i\varphi/2} c_{\vec{k}\uparrow-} - e^{+i\varphi/2} c_{-\vec{k}\downarrow-}^\dagger \right). \quad (15c)$$

In the basis of Bogoliubov quasiparticles $d_{\vec{k}}$ and $f_{\vec{k}}$, the Hamiltonian H_- thus takes a similar form to a normal Weyl semimetal upon replacing $m \rightarrow m \pm |\Delta|$.

The subspace corresponding to $\tau^z = +1$ can be analyzed in the same way, which leads to a Hamiltonian

$$\mathcal{H}_+^{\pm\Delta} = v_F (\hat{z} \times \vec{\sigma}) \cdot \vec{k} + M_+^{\pm\Delta}(k_z) \sigma^z, \quad (16)$$

$$M_+^{\pm\Delta}(k_z) = (m \pm |\Delta|) + \sqrt{t_S^2 + t_D^2 + 2t_S t_D \cos(k_z d)}. \quad (17)$$

For $m > |\Delta|$, this subspace is adiabatically connected to the topologically trivial case $m = |\Delta| = 0$, and Weyl nodes can only appear in the $\tau^z = -1$ sector. By analogy to the normal case, we find that for $m > |\Delta|$, the spectrum of Eq. (12) has up to 4 Bogoliubov Weyl nodes of pairwise opposite chiralities at $\vec{k} = (0, 0, \pi/d \pm k_\pm^\Delta)^T$ with

$$k_\pm^\Delta = \frac{1}{d} \arccos \left(1 - \frac{(m \pm |\Delta|)^2 - (t_S - t_D)^2}{2t_S t_D} \right) \quad (18)$$

if the respective conditions

$$m_{c1} < m \pm |\Delta| < m_{c2} \quad (19)$$

are fulfilled. For $m \pm |\Delta| < m_{c1}$, the respective mode is adiabatically connected to the case $m = |\Delta| = 0$ and thus topologically trivial.

If $m < |\Delta|$, each $\vec{\tau}$ sectors contains one topologically trivial mode as well as one mode that potentially has Weyl nodes. The latter now exist in the range

$$m_{c1} < |\Delta| \pm m < m_{c2}, \quad (20)$$

at the same momenta $\vec{k} = (0, 0, \pi/d \pm k_\pm^\Delta)^T$ with

$$k_\pm^\Delta = \frac{1}{d} \arccos \left(1 - \frac{(|\Delta| \pm m)^2 - (t_S - t_D)^2}{2t_S t_D} \right), \quad (21)$$

and the topologically trivial regime is corresponds to $|\Delta| \pm m < m_{c1}$.

III. CHARACTERIZATION OF THE ACCESSIBLE PHASES

Having recast the Weyl superconductor Hamiltonian into a more convenient form, we will now analyze it in detail. For simplicity, we focus on the case $m > |\Delta|$, when all of the interesting physics happens in H_- defined in Eq. (12). As the discussion in the last section implies, the case $m < |\Delta|$ follows upon interchanging the roles of m and $|\Delta|$ and considering different subspaces of the full Hamiltonian.

We first recall some results for the limiting case $|\Delta| \rightarrow 0$, in which a normal Weyl semimetal is recovered (see Fig. 2(a)).⁵ If the Zeeman mass m is small, $m < m_{c1}$, the system is a topologically trivial insulator. When m reaches m_{c1} , two Weyl nodes of opposite chirality appear at $\vec{K} = (0, 0, \pi/d)^T$. Close to these points, $\vec{k} = \vec{K} + \vec{q}$, the dispersion is roughly given by

$$E \approx \pm v_F \vec{\sigma} \cdot \vec{q}, \quad (22)$$

where \pm defines the chirality of the node.

Upon increasing m , the Weyl nodes move in opposite directions along the \hat{k}_z -axis and to the momenta

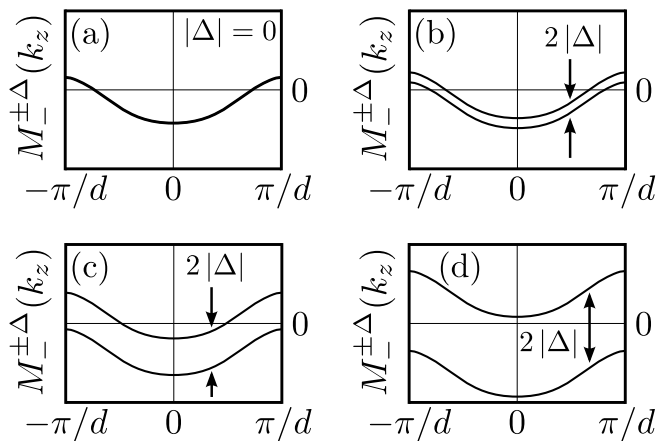


FIG. 2: Evolution of the masses M_{\pm}^{Δ} (upper curve) and M_{\mp}^{Δ} (lower curve) defined in Eq. (14) upon increasing $|\Delta|$. For $|\Delta| = 0$ and $m_{c1} < m < m_{c2}$, the system has two Weyl nodes of chiral electrons, located at the sign changes of M_{\pm}^{Δ} . With superconductivity, each Weyl nodes splits into two Bogoliubov Weyl nodes of equal chirality and opposite particle-hole symmetry. Their separation grows with increasing $|\Delta|$ from subfigures (a) to (d).

$\vec{k} = (0, 0, \pi/d \pm k_{\pm}^{\Delta=0})^T$. For fixed k_z , the combined Hamiltonians $\mathcal{H}_{\pm}^{\pm\Delta=0}$ describe a gapped 2-dimensional Dirac electron. The mass of the latter changes sign at the Weyl nodes. The sign change in the Dirac mass signals a quantum Hall transition. For small $|k_z|$, where the mass is negative, the system is still in the topologically trivial regime. The 2-dimensional systems corresponding to momenta outside the Weyl nodes, however, are in topologically nontrivial quantum Hall state. Chiral surface modes appear on any surface that is not perpendicular to \hat{z} for each value of k_z between the Weyl nodes. This restriction gives rise to so-called Fermi arcs.

A. Effect of pairing on nodes

When superconductivity is turned on, the Hamiltonian decomposes into two copies of itself, acting on Bogoliubov quasiparticles rather than electrons. This is due to the fact that superconductivity splits each electronic state into a particle-hole symmetric and particle-hole antisymmetric state with an energy separation $\sim 2|\Delta|$. For the Hamiltonian H_{-} , these new states correspond to $d_{\vec{k}}$ and $f_{\vec{k}}$ defined in Eq. (15).

Remarkably, the system does not develop a superconducting gap, but rather each Weyl node splits into two separated Bogoliubov Weyl nodes of opposite particle-hole symmetry (see Fig. 2(b)). Both Bogoliubov Weyl nodes have the same chirality, which is inherited from the initial electronic Weyl node, and in this sense half of the topological charge of the initial Weyl node. The particle-hole symmetric and particle-hole antisymmetric subspaces are decoupled. For fixed k_z , each subspace de-

scribes a spinless $p + ip$ -superconductor, which is known to have both a topologically trivial (“strong pairing”) and non-trivial (“weak pairing”) phase.²⁸ The transition between the strong and weak pairing phases is still marked by the Weyl nodes that separate trivial state at small $|k_z|$ from a non-trivial state at large $|k_z|$.

If superconductivity is further increased, the distance between the particle-hole symmetric and antisymmetric Weyl nodes grows. This increases the topologically non-trivial momentum range for one of them (the $\mathcal{H}_{-}^{+\Delta}$ subspace), and shrinks it for the other one (the $\mathcal{H}_{-}^{-\Delta}$ subspace). For $\mathcal{H}_{-}^{-\Delta}$, the Weyl nodes are pushed back towards $\vec{k} = (0, 0, \pi/d)^T$, where they annihilate. The corresponding subspace is left in the topologically trivial insulating state. The Weyl nodes of $\mathcal{H}_{-}^{+\Delta}$ move towards $\vec{k} = 0$. After their annihilation at the origin, they leave the entire Brillouin zone of this subspace in a topologically nontrivial insulating state. The motion of the Weyl nodes upon increase of $|\Delta|$ is followed in Fig. 2. Specifically, subfigure (b) depicts the situation where both subspaces have topologically trivial and nontrivial momenta. Subfigure (c) corresponds to an order parameter amplitude $|\Delta|$ large enough to trivially gap out the $\mathcal{H}_{-}^{-\Delta}$ subspace, while the $\mathcal{H}_{-}^{+\Delta}$ subspace still has Weyl nodes. Subfigure (d) corresponds to even larger $|\Delta|$, such that all Weyl nodes have annihilated.

B. Majorana surface states

For the topologically non-trivial momentum range of k_z , surface states are expected. We model a surface perpendicular to \hat{y} by replacing m and $|\Delta|$ by some smooth functions of y with $m(y), |\Delta|(y) = \text{const.}$ for $y < 0$, and $m(y), |\Delta|(y) \rightarrow 0$ for $y \rightarrow +\infty$ (which realizes a trivial insulator equivalent to the vacuum). The Hamiltonian

$$\mathcal{H}_{-}^{\pm\Delta} = v_F \left(k_x \sigma^y + i \frac{\partial}{\partial y} \sigma^x \right) + M_{\pm}^{\pm\Delta}(k_z, y) \sigma^z \quad (23)$$

indeed has eigenstates

$$\Psi_{\text{surf}}(k_x, k_z, y) = \frac{1}{\mathcal{N}} e^{\int_0^y dy' M_{\pm}^{\pm\Delta}(k_z, y')/v_F} \begin{pmatrix} e^{-i\pi/4} \\ e^{i\pi/4} \end{pmatrix} \quad (24)$$

which are normalizable and exponentially localized at the surface only for momenta k_z with $M_{\pm}^{\pm\Delta}(k_z) > 0$ inside the sample, as anticipated. \mathcal{N} is the corresponding normalization factor. The dispersion of the surface state is linear, $E = v_F k_x/2$.

The “Majorana-ness” of this state can be understood by counting. In particular, recall that the Nambu construction, Eq. (11), nominally doubles the number of components of the fermionic fields. This implies that $\psi_{\vec{k}}$ and $\psi_{-\vec{k}}$ are not independent. Thus corresponding to Eq. (24) there is *one* state, i.e. one canonical (complex) fermion, for each momentum satisfying the localization

condition $M_{\pm}^{\pm\Delta}(k_z) > 0$ with, say, $k_x > 0$, where the last condition is made to keep the states independent. Equivalently, we can divide this complex fermion into two real ones, and associate one real *Majorana* fermion with each k_x , with no restrictions on k_x .

In conclusion, we find that the Bogoliubov Hamiltonians $\mathcal{H}^{+\Delta}$ and $\mathcal{H}^{-\Delta}$ essentially each describe half of a normal Weyl semimetal. They are subject to respective effective Zeeman gaps $m \pm |\Delta|$. A pair of Bogoliubov Weyl nodes of opposite chirality exists if $m_{c1} < m \pm |\Delta| < m_{c2}$. In the sense that two Bogoliubov Weyl nodes arise from a single normal Weyl one, each of the former carries half of the topological charge of the latter. However, this notion is tied up with the non-independence of Bogoliubov states. The corresponding quasiparticles are characterized by their chirality and particle-hole symmetry rather than just chirality in the non-superconducting case. The Bogoliubov Weyl nodes are located at momenta $\vec{k} = (0, 0, k_z)^T$, with

$$M_{\pm}^{\pm\Delta}(k_z) = 0. \quad (25)$$

The vanishing of $M_{\pm}^{\pm\Delta}(k_z)$ reflects a topological transition, regarding the quasiparticles as two dimensional ones parametrized by k_z . For any k_z that satisfies

$$M_{\pm}^{\pm\Delta}(k_z) > 0, \quad (26)$$

the respective Hamiltonian $\mathcal{H}_{\pm}^{\pm\Delta}$ maps to a topologically non-trivial spinless $p+ip$ superconductor and has a chiral surface mode. The latter describes a Majorana particle with linear dispersion perpendicular to \hat{z} and the surface, $E = v_F \vec{k} \cdot (\hat{e}_{\perp} \times \hat{z})/2$. The spin of the surface mode is locked to the direction of propagation. Negative values of $M_{\pm}^{\pm\Delta}(k_z)$, on the contrary, correspond to a trivial insulator.

C. Topological phase diagram

The Hamiltonians $\mathcal{H}_{\pm}^{\pm\Delta}$ can separately be tuned from a topologically trivial to topologically non-trivial state by changing both m and $|\Delta|$. In our model, these two parameters can be tuned separately, although a finite magnetization can in principle affect the proximity induced superconductivity in the TI/SC interfaces. An analysis of the effect of the magnetization on the gap (and of the superconductivity on the magnetic ordering) requires a theory of the superconducting mechanism, like BCS theory, which goes well beyond the treatment here and we think deserves a separate study from this manuscript.

If we exclude a substantial magnetic field due to magnetic impurities, they could most importantly affect the superconductivity in the TI/SC interfaces by an exchange coupling of the nearby superconductor layers to the magnetic impurities. A weakening of the superconductivity there would in turn diminish the proximity effect at the interfaces. Since however the superconductor layers are

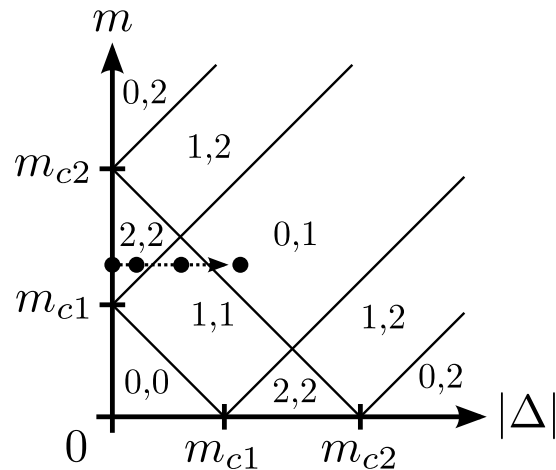


FIG. 3: Phase diagram of a Weyl superconductor in a TI/SC heterostructure as a function of Zeeman gap m and proximity induced superconducting order parameter amplitude $|\Delta|$. The values of m_{c1} and m_{c2} are set by the tunneling amplitudes between the surface Dirac layers of the heterostructure depicted in Fig. 1, see Eq. (10). Each phase is characterized by n_b , the number of pairs of bulk Bogoliubov Weyl nodes, and n_s , the number of two-dimensional Majorana surface modes. The phases are labeled as n_b, n_s . The black dots locate the different subfigures of Fig. 2.

separated from the magnetic impurities by the interfaces, the exchange coupling of the SC to the magnetic impurities is certainly much weaker than the Zeeman term in the interfaces. It is therefore reasonable to neglect the explicit dependence of Δ from m . Similarly, a proximity effect of the SC on the impurities potentially weakening their ferromagnetic ordering is disregarded. This approximation would break down if either the magnetic field of the impurities was important, or if the tunnel coupling between the superconductor and the magnetic impurities was strong.

Neglecting their weak interdependence, a simultaneous modification of m and $|\Delta|$ allows to access a number of different phases with $n_b = 0, 1, 2$ pairs of Bogoliubov Weyl nodes in the bulk and $n_s = 0, 1, 2$ two-dimensional Majorana surface modes (potentially living in a restricted k_z -range). Fig. 3 shows the phase diagram as a function of m and $|\Delta|$, the phases are labeled according to their values of (n_b, n_s) . The phase diagram is mirror symmetric for negative values of m . The tunability of Weyl superconductors (which can be mapped to four copies of a spinless $p+ip$ superconductor per value of k_z , only two of which are potentially topologically non-trivial) is similar to the one of superconducting quantum anomalous Hall insulators (which can be mapped to two topologically potentially non-trivial copies of a spinless $p+ip$ superconductor), although the increased complexity leads to a richer phase diagram for Weyl superconductors.²⁹ Of particular interest are the phases (0,1), which corresponds to a truly topological superconductor (in class D and thus with two-dimensional topological invariants similarly to

a three-dimensional quantum anomalous Hall state), and (1, 1), which is precisely half of a normal Weyl semimetal. We will analyze them further in the next section.³⁰

IV. VORTICES IN WEYL SUPERCONDUCTORS

One of the most interesting features of two dimensional topological superconductors is that they may host a zero energy Majorana mode localized around a vortex. Collections of such Majorana bound states allow for non-local storage of quantum information, which may make the stored information less sensitive to decoherence.³¹ This motivates the analysis of vortices in Weyl superconductors. We specifically discuss the behavior of vortices in the simplest (0, 1) and (1, 1) phases of Fig. 3, which minimize the number of surface Majorana modes. The vortex physics in other phases is qualitatively similar, but may involve more Majorana modes.

The suppression of superconductivity inside a vortex puts its core in either the (0, 2), (2, 2) or (0, 0) phase. For simplicity, we consider the core to be in the trivially insulating (0, 0) phase. In general, the finite size of the core suggests that in any case the core cannot be sharply distinguished from a trivial state, in a full treatment. The (0, 0) state can always be realized for an appropriate choice of m and $|\Delta|$. Nevertheless, our results are not affected by this assumption. Different values of m and $|\Delta|$ will at most change the number and/or direction of propagation of the interface Majorana modes.

Because the heterostructure has one special direction, namely the \hat{z} -axis along which the different layers are stacked, vortices parallel and perpendicular to \hat{z} have to be distinguished, as depicted in Fig. 4. The qualitative physics of vortices can be understood by analogy to ³He-A, which also is a Weyl superconductor.^{2,32} As pointed out in Ref. 32, the momentum range in which Majorana bound states at a vortex exist is proportional to $\hat{e}_v \cdot \hat{z}$, where \hat{e}_v is the direction of the vortex. In particular, a vortex perpendicular to \hat{z} has no bound states. In the following, we will analyze the behavior of vortices in TI/SC heterostructures in more detail.

A. Vortex along the superlattice axis

At first, we turn to a magnetic field \vec{B} applied along \hat{z} , the stacking axis of the heterostructure. For modest field strengths, only few vortices are present, and interactions between vortices can be neglected. This situation is sketched in Fig. 4(a). By assumption, the vortex core is in a topologically trivial insulating state. The boundary of the vortex is thus equivalent to an interface between a Weyl superconductor and vacuum and has 1 Majorana edge mode. If the Weyl superconductor is in the (1, 1) phase, this mode has a restricted range of momenta k_z (it lives "between the Bogoliubov Weyl nodes"), the (0, 1)

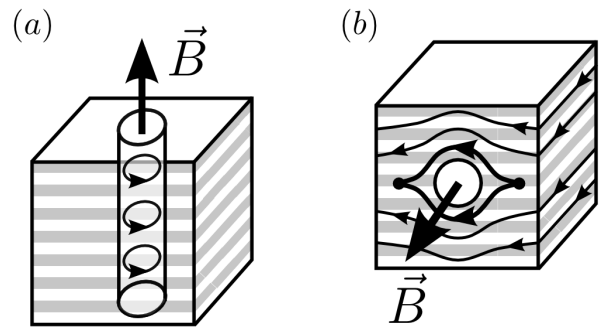


FIG. 4: The two classes of vortices in Weyl superconductors. Subfigure (a) sketches a vortex along the superlattice axis \hat{z} , with bound states along a tube through the whole sample. Subfigure (b) depicts a vortex perpendicular to \hat{z} . Whereas there are no states bound to the vortex, the surface states can be used for Majorana interferometry (thick line).

phase has interface modes for any momentum k_z . We restrict the discussion to $|\Delta| < m$ when all relevant physics happens in H_- , but the results can easily be generalized.

Exploiting the cylindrical symmetry with respect to the vortex axis, we model the latter by a radially dependent Zeeman gap m and superconducting order parameter $\Delta(\vec{r}) = |\Delta(r)|e^{i\varphi(\phi)}$, where $\varphi(\phi) = \varphi_0 - (\Phi/\Phi_0)\phi$ is the phase of the order parameter. The latter is now twisted due to the presence of a magnetic field (ϕ denotes the angular coordinate). The twist is proportional to the flux Φ trapped by the vortex, which itself is quantized in units of $\Phi_0 = hc/2e = \pi/e$, as usual for superconductors. The phase φ_0 corresponds to the superconducting phase without magnetic field. The radius of the vortex is considered to be R , and $m(r)$ and $|\Delta(r)|$ are smooth functions interpolating between fixed values m and $|\Delta|$ for $r > R$, and $|m| < m_{c1}$, $|\Delta| = 0$ inside the core of the vortex. The magnetic field is $\vec{B} = B\hat{z}$ inside the vortex and for simplicity assumed to vanish everywhere else. This gives rise to a vector potential

$$\begin{aligned} \vec{A}(\vec{r}) &= A(r) \hat{e}_\phi, \\ A(r) &= \frac{Br}{2} \Theta(R-r) + \frac{BR^2}{2r} \Theta(r-R) \end{aligned} \quad (27)$$

in \hat{e}_ϕ direction, that is taken into account by minimal coupling $\vec{k} \rightarrow \vec{k} - e\vec{A}$ in the Hamiltonian (1). After a canonical transformation $\sigma^x \rightarrow -\sigma^y$, $\sigma^y \rightarrow \sigma^x$, the rele-

vant Hamiltonian H_- in Eq. (11) becomes

$$H_- = \sum_{k_z} \int d^2r \psi_{k_z}^\dagger(\vec{r}) \mathcal{H}_- \psi_{k_z}(\vec{r}), \quad (28a)$$

$$\mathcal{H}_- = \begin{pmatrix} \mathcal{H}_A & |\Delta(r)| e^{i\varphi(\phi)} \sigma^z \\ |\Delta(r)| e^{-i\varphi(\phi)} \sigma^z & \mathcal{H}_{-A} \end{pmatrix}, \quad (28b)$$

$$\begin{aligned} \mathcal{H}_A = M_-(k_z, r) \sigma^z + v_F & \begin{pmatrix} 0 & -i e^{-i\phi} \\ -i e^{i\phi} & 0 \end{pmatrix} \frac{\partial}{\partial r} \\ + v_F & \begin{pmatrix} 0 & -e^{-i\phi} \\ e^{i\phi} & 0 \end{pmatrix} \left(\frac{1}{r} \frac{\partial}{\partial \phi} + i e A(r) \right). \end{aligned} \quad (28c)$$

For any given k_z , this Hamiltonian may be interpreted as two copies of a spinless $p+ip$ superconductor threaded by a magnetic flux. By analogy, the vortex binds one Majorana zero mode per topological value of k_z and per topological subsector if it traps an odd number of flux quanta, and no zero mode for an even number of trapped flux quanta.²⁸ Assuming that there is only a single topologically non-trivial subsector, one can thus define a unique zero energy Majorana mode bound to the vortex. See appendix B for more details.

Physically, the Majorana bound state can be understood in terms of an Aharonov-Bohm like phase, a Berry phase and a geometrical phase for the Majorana surface states. Consider the topologically equivalent situation of a Weyl superconductor with a tube-like hole along the \hat{z} axis. Without a magnetic field inside the hole, we know that chiral Majorana surface states exist when k_z is chosen in the range where the two-dimensional superconductor is in the topological phase. Since the spin is locked to the momentum, the surface states pick up a Berry phase of π upon encircling the hole once. This shifts the zero momentum mode away from zero energy and can be interpreted as effectively antiperiodic boundary condition on the geometrical phase in order to counterbalance the Berry phase. If now a unit flux is threaded through the tube-like hole, the surface states pick up an additional phase of π . The latter derives from the winding of the order parameter phase, and is similar to an Aharonov-Bohm effect. It compensates the Berry phase and thus allows for zero energy bound states. Similar effects have also been discussed for confined magnetic flux tubes imposed in 3-dimensional strong topological insulators.^{34,35} For momenta k_z which are in the topologically trivial range, of course, no bound states exist both with and without magnetic flux. Because the magnetic field vanishes outside the vortex, the topological character and especially the existence of surface states is unchanged there. We thus conclude that a vortex with an odd number of flux quanta traps a Majorana zero mode for every topologically non-trivial value of k_z .

In a more realistic model, the Majorana bound states do not form totally flat bands as a function of k_z . The presence of a zero energy Majorana mode for odd-integer fluxes is however partially robust. As an effective model at lowest energies, we consider the zero energy band of

Majorana modes as a function of k_z . After transforming to Wannier orbitals, we obtain a set of Majorana bound states at different heights z , as depicted in Fig. 4(a). This Hamiltonian can be interpreted as a 1-dimensional chain of decoupled sites. Next, we introduce a small hopping along the chain, thus allowing the Majoranas to move up and down the vortex tube. In dimensionless units, their dispersion is given by

$$E = -\cos(k_z). \quad (29)$$

Therefore, zero energy Majorana bound states exist if

1. a Majorana bound state can be defined for $k_z = \pm\pi/2$, i.e. $M_-^{\pm\Delta}(\pm\pi/2) > 0$, and if
2. k_z can take the values $\pm\pi/2$.

The first condition is always fulfilled in the (0,1) phase, but depends on the exact position of the Bogoliubov Weyl nodes in the (1,1) phase. The second condition depends on the number of layers of the TI/SC heterostructure and the boundary conditions. Choosing for instance hard wall boundary conditions, one finds exactly one zero energy Majorana mode if the system has an odd number of superlattice layers, and no zero energy Majorana modes for an even number of layers. This result is quite natural, in a weak tunneling picture. Majorana states in a pair of layers can mix to form a Dirac fermion, moving away from zero energy. Only for an odd number of layers is an unpaired Majorana left behind at zero energy.

B. Vortex perpendicular to the superlattice axis

Viewing the vortex, as in the previous subsection, as a cylindrical hole enclosing a flux, the discussion in Sec. III B implies that a vortex perpendicular to the axis \hat{z} of the heterostructure should also host Majorana modes. In our model, they run between the front and back surfaces of the heterostructure on the side walls of the vortex. For a thin vortex, however, already a small coupling across the flux line is sufficient to hybridize and consequently gap out these two states. We thus recover the result of Ref. 32.

The hole comprising the vortex also introduces a new edge at the sample boundary (the circular ends of the cylindrical hole). The nearby surface states will rearrange in order to host the vortex and locally run along this new edge, as depicted in Fig. 4(b). While there are no states bound to the vortex, a special class of surface state paths allows for Majorana interferometry, depicted by thick lines in Fig. 4(b). It may be interesting to study experimental measurements of interference in such structures.

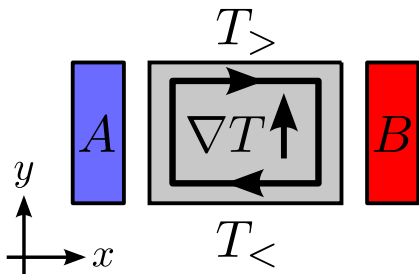


FIG. 5: Sketch of the anomalous thermal Hall effect in Weyl superconductors. The sample is shown from above. A thermal gradient ∇T is applied across the sample. The upper surface is at a temperature $T_>$ larger than the temperature $T_<$ of the lower surface. This leads to a net heat current from side A to side B perpendicular to the temperature gradient transported by the surface modes running around the sample.

V. EXPERIMENTAL PROBES

A. Anomalous thermal Hall effect

Because Majorana particles do not carry electric charge, a natural way to measure surface Majorana states is to detect their thermal transport. We again focus on a Weyl superconductor in the (0,1) or (1,1) phase. As there is only a single Majorana surface modes, these phases should exhibit only half of the thermal transport of a normal Weyl semimetal in the corresponding regime.

On a surface perpendicular to \hat{y} , thermodynamics can be calculated from the effective Majorana surface partition function

$$Z = \int \mathcal{D}(\bar{\Psi}_{\omega_n, k_x, k_z}, \Psi_{\omega_n, k_x, k_z})_{k_x > 0} e^{-\mathcal{S}}, \quad (30)$$

$$\mathcal{S} = \sum_{\substack{\omega_n, \\ k_x > 0, k_z}} \bar{\Psi}_{\omega_n, k_x, k_z} (-i\omega_n + v_F k_x) \Psi_{\omega_n, k_x, k_z}, \quad (31)$$

where the operators $\Psi_{\omega_n, k_x, k_z}^\dagger$ create excitations above the Bogoliubov vacuum. Note the restriction to $k_x > 0$, which is because pairs of Majorana fermions at k_x and $-k_x$ have been recombined into the canonical Ψ fermion (c.f. Sec. III B).

If a thermal gradient ∇T is applied across the Weyl semimetal, each surface mode transports heat only in its direction of propagation. Therefore, the thermal gradient leads to a net heat transport perpendicular to ∇T , as depicted in Fig. 5. This phenomenon is known as the thermal Hall effect. It has been proposed as an experimental signature of various other chiral edge states, for example in the spin Hall effect, the fractional quantum Hall effect or topological superconductors.^{28,37–39} We presume any bulk transport to be parallel to the gradient, so that it can be separated from the surface contribution. In any case, the dependence upon field, density, etc. of any possible bulk contribution would be very different from that of the surface one.

For concreteness, consider a temperature gradient ∇T imposed across the sample in the \hat{y} direction. This leads to a net difference in the distribution of quasiparticles on the $y = 0$ and $y = L_y$ surfaces. The result is an excess heat current I_Q , in the x direction, which defines the thermal Hall conductance K_{xy} , according to

$$I_Q = K_{xy} |\nabla T|. \quad (32)$$

For small temperature differences between the surfaces, the excess heat current is obtain by differentiation, and we obtain

$$K_{xy} = \sum_{k_z} \int_0^\infty \frac{dk_x}{2\pi} v_F^2 k_x \frac{\partial n_F(v_F k_x)}{\partial T}, \quad (33)$$

$$= \sum_{k_z} \frac{1}{2} \frac{k_B^2 \pi^2 T}{3h}, \quad (34)$$

with k_z being summed over all topologically non-trivial values for the given phase of the Weyl superconductor (either (0,1) or (1,1)) and n_F denoting the Fermi-Dirac distribution at the temperature T . Note that we have restored physical units such as Boltzmann's constant k_B and Planck's constant h for concreteness. As expected, the surface of a Weyl superconductor has half of the thermal Hall conductance of a quantum Hall edge state per allowed momentum k_z . This is not surprising because the thermal Hall coefficient is proportional to the central charge c of the surface modes, $K_{xy} = c \pi^2 k_B^2 T / (3h)$, similar to the heat capacity.^{28,40}

Coming back to the Weyl superconductor in the (0,1) or (1,1) phase, the thermal Hall effect has an anomalous coefficient proportional to the distance $2k_+^\Delta$ between the Weyl nodes defined in Eq. (18). Concretely, the thermal Hall conductance is proportional to the length of the system in the \hat{z} direction, $K_{xy} = \kappa_{xy} L_z$, with

$$\kappa_{xy} = \frac{1}{2} \frac{k_B^2 \pi^2 T}{3h} \frac{k_+^\Delta}{\pi}. \quad (35)$$

In the (0,1) phase, where $k_+^\Delta = \pi/d$, each TI layer contributes the full Majorana quantum $(1/2) \pi^2 k_B^2 T / (3h)$ to the thermal Hall coefficient. Although thermal transport measurements are experimentally demanding, the higher dimensionality of the surface states in a Weyl superconductor as compared to fractional or spin quantum Hall edge states hopefully tends to result in more approachable experiments.

B. Electrical transport

As discussed in Sec. III, the surface physics of a Weyl superconductor can be understood as layers of spinless $p+ip$ superconductors stacked in momentum space along k_z , with potentially associated edge states. In order to minimize bulk transport, we now specialize to the (0,1) phase. The surface of the Weyl superconductor is then

equivalent to just one non-trivial spinless $p + ip$ superconductor edge state per value of k_z . In this phase, electric transport experiments that have been proposed for $p + ip$ superconductors can simply be transferred to Weyl superconductors. The general idea is to bring different samples with Majorana edge modes into contact. Whenever an interface has two edge modes running into the same direction, electrons can tunnel into the interface by decomposition in the two Majorana particles. These two Majorana particles can then be transported in parallel, giving rise to a one-directional electronic transport channel along the interface.⁴¹ In alternative setups, the two Majoranas can be separated and recombined with different Majorana modes, which leads to distinct signatures in conductance and noise.⁴² The latter experiments are however less appropriate for Weyl superconductors where each surface has a large number of generically coupled Majorana modes at different values of k_z .

VI. SUMMARY AND CONCLUSIONS

We have shown how a variety of gapless and/or topological superconducting phases can be achieved in superconducting-topological insulator superlattices. These phases are analogous to quasiparticle states of ^3He . The most interesting $(0, 1)$ and $(1, 1)$ phases exhibit Majorana surface states on some surfaces, and bound to the cores of vortices. Particularly in the gapless phases, such as $(1, 1)$, these Majorana states exist only for a range of momenta, k_z , along the modulated direction of the superlattice. In such a case, no local (in z) description of the Majorana modes is possible, as opposed to the situation in the $(0, 1)$ phase, in which the Majorana modes can be modeled in terms of a real-space tight-binding Hamiltonian in the z direction, and the state can be considered as a sort of stack of two-dimensional topological superconductors.

It is hoped that the proposed structures might be explored experimentally in the future. While we do not discuss materials in any detail here, we note that recent studies have shown that $\text{Cu}_x\text{Bi}_2\text{Se}_3$ ^{25–27} becomes a superconductor with $x \approx 0.14$, while it is a topological insulator for $x = 0$, so that a superlattice with modulated x might be a candidate realization of this proposal. Some *ab initio* modeling of such a superlattice would probably be useful prior to any experimental attempts. Alternatively, spin-triplet superconductors have recently been identified to exhibit Weyl superconducting phases as well.^{43,44}

There is significant scope for further theoretical study of Weyl and topological superconductors in three dimensions. The Majorana surface states of $(0, 1)$ and $(1, 1)$ phases are rather analogous to the “chiral surface sheaths” which occur in three-dimensional quantum Hall systems,^{45,46} where interesting vertical transport, quantum interference, and universal conductance fluctuations have been studied, and it would be interesting to see

how such phenomena translate to the superconducting case. We have also not touched on the Adler-Bell-Jackiw anomaly associated with Weyl points. This has been discussed recently for normal Weyl semimetals, where it may lead to anomalous magnetotransport.⁷ It is not obvious what the consequences are for Weyl superconductors. One might also consider Josephson effects for currents along the z axis. We leave these questions for future work.

Acknowledgments

We acknowledge discussions with Victor Galitski, and Xiaoliang Qi. L.B. was supported by NSF grants DMR-0804564 and PHY05-51164. T.M. gratefully acknowledges the hospitality of KITP, where part of this work was done, as well as financial support by SFB 608 and FOR 960 of the DPG, and the Bonn-Cologne graduate school (BCGS).

Appendix A: Gaplessness of inversion symmetric Weyl superconductors

In this appendix, we discuss the qualitative behavior of Weyl semimetals under superconducting proximity effect. We assume that either time reversal or inversion symmetry is conserved, while the respective other symmetry needs to be broken for the system to exhibit Weyl physics. As has been mentioned in the introduction, the fate of the Weyl superconductor depends on which of the symmetries is conserved. For inversion symmetric, time reversal symmetry broken Weyl semimetals, the presence of a Weyl node at \vec{k}_0 implies the presence of a Weyl node of *opposite* chirality at $-\vec{k}_0$. In Weyl semimetals with broken inversion symmetry, however, time reversal symmetry guarantees the presence of Weyl nodes of *equal* chirality at $\pm\vec{k}_0$. When a superconducting proximity effect is turned on, the low energy modes at these two Weyl nodes mix. However, the superconducting correlations more precisely couple electrons on one Weyl node to holes on the other, instead of electrons to electrons as a more standard perturbation would do. This effectively inverts the chirality of one of the Weyl nodes. Consequently, the proximity effect in inversion symmetric systems *effectively* mixes Weyl nodes of the *same* chirality, and no gap opens. In time reversal symmetric systems, on the contrary, the mixed Weyl nodes effectively have *opposite* chiralities, and a gap is to be expected.

To be more concrete, we consider the effective low energy theory of a Weyl semimetal, which corresponds to electrons living close to Weyl nodes. Since standard superconductivity couples electrons at momenta $\pm\vec{k}$, we focus our effective model on two of the Weyl nodes located at momenta $\pm\vec{k}_0$. For an inversion symmetric system, where the nodes are of opposite chirality, this already

describes a complete minimal model. For a time reversal symmetric system, the nodes at $\pm\vec{k}_0$ have the same chirality, and there must exist at least two additional nodes, say at $\pm\vec{k}_1$, of the respective opposite chirality. Since these two pairs of nodes are decoupled, we can understand the system as two copies of the following Hamiltonian (A4) describing only two Weyl nodes. The latter thus allows us to decide on the presence or absence of a gap.

As advertized, our result will only depend on whether the two initial Weyl nodes have the same or opposite chirality. We therefore assume one Weyl node to have positive chirality, $H_1 \sim \vec{\sigma} \cdot \vec{k}$, while the second node is so far keep in a general notation, $H_2 \sim \pm \vec{\sigma} \cdot \vec{k}$ in order to tackle both the time reversal symmetric and inversion symmetric cases simultaneously. The electrons close to these nodes are described by the operators $c_{1,\vec{k},\sigma}$ and $c_{2,\vec{k},\sigma}$, respectively. We furthermore measure the momenta relative to the respective Weyl nodes, such that the non-superconducting Hamiltonian reads

$$\begin{aligned} H_0 &= \sum_{\vec{k}} (c_{1,\vec{k},\uparrow}^\dagger, c_{1,\vec{k},\downarrow}^\dagger) (v_F \vec{\sigma} \cdot \vec{k}) \begin{pmatrix} c_{1,\vec{k},\uparrow} \\ c_{1,\vec{k},\downarrow} \end{pmatrix} \quad (\text{A1}) \\ &+ \sum_{\vec{k}} (c_{2,\vec{k},\uparrow}^\dagger, c_{2,\vec{k},\downarrow}^\dagger) (\pm v_F \vec{\sigma} \cdot \vec{k}) \begin{pmatrix} c_{2,\vec{k},\uparrow} \\ c_{2,\vec{k},\downarrow} \end{pmatrix} \\ &= \sum_{\vec{k}} \Psi_{\vec{k},0}^\dagger \begin{pmatrix} v_F \vec{\sigma} \cdot \vec{k} & 0 \\ 0 & \pm v_F \vec{\sigma} \cdot \vec{k} \end{pmatrix} \Psi_{\vec{k},0} \end{aligned}$$

with $\Psi_{\vec{k},0} = (c_{1,\vec{k},\uparrow}, c_{1,\vec{k},\downarrow}, c_{2,\vec{k},\uparrow}, c_{2,\vec{k},\downarrow})^T$. We assume that the superconducting part of the Hamiltonian only contains terms of the form

$$H_{SC} \sim h(\vec{k}) c_{1,\vec{k},\sigma}^\dagger c_{2,-\vec{k},\sigma'}^\dagger + \text{h.c.}, \quad (\text{A2})$$

which in particular includes s-wave and p-wave pairing. It is now useful to rewrite the non-superconducting part of the Hamiltonian as

$$H_0 = \sum_{\vec{k}} \Psi_{\vec{k},\Delta}^\dagger \begin{pmatrix} v_F \vec{\sigma} \cdot \vec{k} & 0 \\ 0 & \mp v_F \vec{\sigma} \cdot \vec{k} \end{pmatrix} \Psi_{\vec{k},\Delta}, \quad (\text{A3})$$

where $\Psi_{\vec{k},\Delta} = (c_{1,\vec{k},\uparrow}, c_{1,\vec{k},\downarrow}, c_{2,-\vec{k},\downarrow}^\dagger, -c_{2,-\vec{k},\uparrow}^\dagger)^T$. We note that the sign of the second Weyl node in the Hamiltonian has to be reversed due to the inversion of creation and annihilation operators. This precisely corresponds to the effective inversion of the chirality of the second node under proximity effect, see above. Including a general superconducting term, the full Hamiltonian $H = H_0 + H_{SC}$

can be written as

$$\begin{aligned} H &= \sum_{\vec{k}} \Psi_{\vec{k},\Delta}^\dagger \mathcal{H} \Psi_{\vec{k},\Delta}, \quad (\text{A4}) \\ \mathcal{H} &= \begin{pmatrix} v_F \vec{\sigma} \cdot \vec{k} & [\alpha(\vec{k}) \mathbf{1}_\sigma + \vec{\beta}(\vec{k}) \cdot \vec{\sigma}] \\ [\alpha(\vec{k})^* \mathbf{1}_\sigma + \vec{\beta}(\vec{k})^* \cdot \vec{\sigma}] & \mp v_F \vec{\sigma} \cdot \vec{k} \end{pmatrix}. \quad (\text{A5}) \end{aligned}$$

For an inversion symmetric system, where the lower (plus) sign applies, the diagonal is proportional to the unit matrix in Nambu space. Superconductivity can therefore never open up a gap, but only shift the Bogoliobov Weyl nodes in momentum space. For time reversal symmetric systems, the Hamiltonian is however generically gapped. As an example, we consider s-wave superconductivity. The latter corresponds to

$$\begin{aligned} H_{\text{s-wave}} &= \sum_{\vec{k}} \Delta c_{1,\vec{k},\uparrow}^\dagger c_{2,-\vec{k},\downarrow}^\dagger + \text{h.c.} \quad (\text{A6}) \\ &= \sum_{\vec{k}} \frac{\Delta}{2} (c_{1,\vec{k},\uparrow}^\dagger c_{2,-\vec{k},\downarrow}^\dagger - c_{2,\vec{k},\downarrow}^\dagger c_{1,-\vec{k},\uparrow}^\dagger) + \text{h.c.}, \end{aligned}$$

where we neglect the superconducting phase for simplicity, i.e. $\Delta = |\Delta|$. The total Hamiltonian then reads

$$H = \sum_{\vec{k}} \Psi_{\vec{k},\Delta}^\dagger \begin{pmatrix} v_F \vec{\sigma} \cdot \vec{k} & \frac{\Delta}{2} \mathbf{1}_\sigma \\ \frac{\Delta}{2} \mathbf{1}_\sigma & -v_F \vec{\sigma} \cdot \vec{k} \end{pmatrix} \Psi_{\vec{k},\Delta}. \quad (\text{A7})$$

The eigenvalues of this Hamiltonian are easily found as

$$E = \pm \sqrt{(v_F \vec{\sigma} \cdot \vec{k})^2 + \frac{|\Delta|^2}{4}}, \quad (\text{A8})$$

and the system is gapped as expected. Finally, consider adiabatically restoring inversion symmetry. Throughout this process, superconductivity ensures the system to be gapped. A time reversal symmetric, inversion symmetry broken Weyl superconductor can thus adiabatically be connected to the trivial state respecting both symmetries, and is therefore a trivial insulator itself.

Appendix B: Expression of the zero energy Majorana bound state

A vortex in a Weyl superconductor traps a unique zero energy bound state if it contains an odd number of flux quanta. To explicitly show this, let us first discuss the bound state for a simple limiting case where the algebra can be done explicitly, and then turn to the general solution.

The limiting case is defined as follows. We assume that the Zeeman mass m is constant in the entire Weyl superconductor (and in particular takes the same value inside and outside the vortex). Moreover, we assume

that $m_{c_1} < m < m_{c_2}$, such that there is one momentum $k_z = k_z^0$ with $M_-(r, k_z^0) = 0$ everywhere. As follows from Fig. 3, we are then able to find a $|\Delta| = \Delta_0$ outside the vortex such that only one subsector is topologically non-trivial, and expect a single zero energy Majorana mode bound to the vortex for this choice of $|\Delta|$. In addition, we assume that there is only a single flux quantum inside the vortex. Outside the vortex, the Hamiltonian (28) reads for $k_z = k_z^0$

$$H_- = \int_{r>R} d^2r \psi_{k_z^0}^\dagger(\vec{r}) \mathcal{H}_- \psi_{k_z^0}(\vec{r}), \quad (\text{B1a})$$

$$\mathcal{H}_- = \begin{pmatrix} \mathcal{H}_B & |\Delta(r)| e^{i\varphi(\phi)} \sigma^z \\ |\Delta(r)| e^{-i\varphi(\phi)} \sigma^z & \mathcal{H}_{-B} \end{pmatrix}, \quad (\text{B1b})$$

$$\begin{aligned} \mathcal{H}_B &= v_F \begin{pmatrix} 0 & -i e^{-i\phi} \\ -i e^{i\phi} & 0 \end{pmatrix} \frac{\partial}{\partial r} \\ &+ v_F \begin{pmatrix} 0 & -e^{-i\phi} \\ e^{i\phi} & 0 \end{pmatrix} \left(\frac{1}{r} \frac{\partial}{\partial \phi} + i e \frac{B R^2}{2r} \right). \end{aligned} \quad (\text{B1c})$$

The order parameter amplitude $|\Delta(r)|$ goes to zero in the vortex core and takes the value $|\Delta(r)| = \Delta_0$ far away from the vortex. For $k_z = k_z^0$, this Hamiltonian has two linearly independent normalizable zero energy bound state solutions,

$$\Psi_1^{\text{outer}} = \frac{1}{\mathcal{N}''} \frac{1}{\sqrt{r}} e^{-\int_R^r dr' |\Delta(k_z^0, r')|/v_F} \begin{pmatrix} e^{-i\phi} \\ 0 \\ 0 \\ i e^{i\phi} \end{pmatrix}, \quad (\text{B2})$$

$$\Psi_2^{\text{outer}} = \frac{1}{\mathcal{N}''} \frac{1}{\sqrt{r}} e^{-\int_R^r dr' |\Delta(k_z^0, r')|/v_F} \begin{pmatrix} 0 \\ i \\ 1 \\ 0 \end{pmatrix}. \quad (\text{B3})$$

Inside the vortex. i.e. for $r < R$, where

$$\begin{aligned} \mathcal{H}_B &= v_F \begin{pmatrix} 0 & -i e^{-i\phi} \\ -i e^{i\phi} & 0 \end{pmatrix} \frac{\partial}{\partial r} \\ &+ v_F \begin{pmatrix} 0 & -e^{-i\phi} \\ e^{i\phi} & 0 \end{pmatrix} \left(\frac{1}{r} \frac{\partial}{\partial \phi} + i e \frac{B r}{2} \right), \end{aligned} \quad (\text{B4})$$

only the state

$$\Psi_2^{\text{inner}} = \frac{1}{\mathcal{N}'''} e^{-1/v_F \int_R^r dr' (|\Delta(k_z^0, r')| + e B r'/2)} \begin{pmatrix} 0 \\ i \\ 1 \\ 0 \end{pmatrix} \quad (\text{B5})$$

is normalizable. The state that would be connected to Ψ_1 is given by

$$\psi_1^{\text{inner}} \sim e^{-1/v_F \int_R^r dr' (|\Delta(k_z^0, r')| + 1/r' - e B r'/2)} \begin{pmatrix} e^{-i\phi} \\ 0 \\ 0 \\ i e^{i\phi} \end{pmatrix}. \quad (\text{B6})$$

This state however diverges at the origin as $\psi_1^{\text{inner}} \xrightarrow{r \rightarrow 0} 1/r$ and is thus *not normalizable*. Consequently, there is only a single normalizable zero energy state bound to the vortex. Up to the normalization, it is given by

$$\Psi = \Psi_2^{\text{inner}} \Theta(R - r) + \Psi_2^{\text{outer}} \Theta(r - R). \quad (\text{B7})$$

When we consider a momentum k_z close to k_z^0 or change the Zeeman gap m a little bit, the system will stay in the same extended topological phase. There will thus always be a single zero energy bound state per topological momentum as long as there is no topological phase transition. We find that the Hamiltonian (28) always exhibits two linearly independent zero energy bound states for $r > R$. For $M_{-\Delta}^+(k_z, r') > 0$ and $M_{-\Delta}^-(k_z, r') < 0$ at large r , they are given by

$$\Psi_{+\Delta}^{\text{outer}} \sim \frac{1}{\sqrt{r}} e^{-\int_R^r dr' M_{-\Delta}^+(k_z, r')/v_F} \begin{pmatrix} e^{-i\phi} \\ i \\ 1 \\ i e^{i\phi} \end{pmatrix} \quad (\text{B8})$$

$$\Psi_{-\Delta}^{\text{outer}} \sim \frac{1}{\sqrt{r}} e^{+\int_R^r dr' M_{-\Delta}^-(k_z, r')/v_F} \begin{pmatrix} e^{-i\phi} \\ -i \\ -1 \\ i e^{i\phi} \end{pmatrix}. \quad (\text{B9})$$

The bound state will be a superposition of these two states that connects to the normalizable solution for $r < R$. The special case considered previously corresponds to $M_{-\Delta}^+ = -M_{-\Delta}^- = |\Delta(r)|$ and $\Psi_2 \sim \Psi_{+\Delta} - \Psi_{-\Delta}$.

¹ C. Herring, Phys. Rev. **52**, 365 (1937).

² G. E. Volovik, *The Universe in a Helium Droplet* (Clarendon Press, Oxford, 2003).

³ X. Wan, A. M. Turner, A. Vishwanath, and S. Y. Savrasov, Phys. Rev. B **83**, 205101 (2011).

⁴ K.-Y. Yang, Y.-M. Lu, and Y. Ran, Phys. Rev. B **84**, 075129 (2011).

⁵ A. A. Burkov, and L. Balents, Phys. Rev. Lett. **107**,

127205 (2011).

⁶ P. Hosur, S. A. Parameswaran, and A. Vishwanath, Phys. Rev. Lett. **108**, 046602 (2012).

⁷ V. Aji, arXiv:1108.4426 (2011).

⁸ A. A. Zyuzin, S. Wu, and A. A. Burkov, Phys. Rev. B **85**, 165110 (2012).

⁹ S. Murakami, New J. Phys. **9**, 356 (2007).

¹⁰ G. Xu, H. Weng, Z. Wang, X. Dai, and Z. Fang,

- Phys. Rev. Lett. **107**, 186806 (2011).
- ¹¹ W. Witczak-Krempa, and Y. B. Kim, Phys. Rev. B **85**, 045124 (2012).
 - ¹² G. Y. Cho, arXiv:1110.1939 (2011).
 - ¹³ S. M. Young, S. Zaheer, J. C. Y. Teo, C. L. Kane, E. J. Mele, and A. M. Rappe Phys. Rev. Lett. **108**, 140405 (2012).
 - ¹⁴ J.-H. Jiang, Phys. Rev. A **85**, 033640 (2012).
 - ¹⁵ P. Delplace, J. Li, and D. Carpentier, Europhys. Lett. **97**, 67004 (2012).
 - ¹⁶ Z. Wang, Y. Sun, X.-Q. Chen, C. Franchini, G. Xu, H. Weng, X. Dai, and Z. Fang, Phys. Rev. B **85**, 195320 (2012).
 - ¹⁷ A. Go, W. Witczak-Krempa, G. S. Jeon, K. Park, Y. B. Kim arXiv:1202.4460 (2012).
 - ¹⁸ A. A. Burkov, M. D. Hook, and L. Balents, Phys. Rev. B **84**, 235126 (2011).
 - ¹⁹ G. B. Halász, and L. Balents, Phys. Rev. B **85**, 035103 (2012).
 - ²⁰ Q. Liu, C.-X. Liu, C. Xu, X.-L. Qi, and S.-C. Zhang, Phys. Rev. Lett. **102**, 156603 (2009).
 - ²¹ R. Yu, W. Zhang, H.-J. Zhang, S.-C. Zhang, X. Dai, and Z. Fang, Science **329**, 61 (2010).
 - ²² D. A. Abanin, and D. A. Pesin, Phys. Rev. Lett. **106**, 136802 (2011).
 - ²³ G. Rosenberg, and M. Franz, Phys. Rev. B **85**, 195119 (2012).
 - ²⁴ J. D. Sau, S. Tewari, R. M. Lutchyn, T. D. Stanescu, and S. Das Sarma, Phys. Rev. B **82**, 214509 (2010).
 - ²⁵ G. Zhang *et al.*, Appl. Phys. Lett. **95**, 053114 (2009).
 - ²⁶ H. Peng *et al.*, Nature Mater. **9**, 225 (2009).
 - ²⁷ Y. Zhang *et al.*, Nature Phys. **6**, 584 (2010).
 - ²⁸ N. Read, and D. Green, Phys. Rev. B **61**, 10267 (2000).
 - ²⁹ X.-L. Qi, T. L. Hughes, and S.-C. Zhang, Phys. Rev. B **82**, 184516 (2010).
 - ³⁰ A. P. Schnyder, S. Ryu, A. Furusaki, and A. W. W. Ludwig, Phys. Rev. B **78**, 195125 (2008).
 - ³¹ A. Y. Kitaev, Phys. Usp. **44** (suppl.), 131 (2001).
 - ³² G. E. Volovik, JETP Lett. **93**, 66 (2011).
 - ³³ L. Fu, and C. L. Kane, Phys. Rev. Lett. **100**, 096407 (2008).
 - ³⁴ G. Rosenberg, H.-M. Guo, and M. Franz, Phys. Rev. B **82**, 041104(R) (2010).
 - ³⁵ C.-K. Chiu, M. J. Gilbert, and T. L. Hughes, Phys. Rev. B **84**, 144507 (2011).
 - ³⁶ L. Fu, and C. L. Kane, Phys. Rev. Lett. **102**, 216403 (2009).
 - ³⁷ C. L. Kane, and M. P. A. Fisher, Phys. Rev. B **55**, 15832 (1997).
 - ³⁸ T. Senthil, J. B. Marston, and M. P. A. Fisher, Phys. Rev. B **60**, 4245 (1999).
 - ³⁹ Z. Wang, X.-L. Qi, and S.-C. Zhang, Phys. Rev. B **84**, 014527 (2011).
 - ⁴⁰ H. W. J. Blöte, J. L. Cardy, and M. P. Nightingale, Phys. Rev. Lett. **56**, 742 (1986); I. Affleck, *ibid.* **56**, 746 (1986).
 - ⁴¹ I. Serban, B. Béri, A. R. Akhmerov, and C. W. J. Beenakker, Phys. Rev. Lett. **104**, 147001 (2010).
 - ⁴² S. B. Chung, X.-L. Qi, J. Maciejko, and S.-C. Zhang, Phys. Rev. B **83**, 100512(R) (2011).
 - ⁴³ J. D. Sau, and S. Tewari, arXiv:1110.4110 (2011).
 - ⁴⁴ Y. Li, and C. Wu, Scientific Report **2**, 392 (2012).
 - ⁴⁵ J. T. Chalker, and A. Dohmen, Phys. Rev. Lett. **75**, 4496 (1995).
 - ⁴⁶ L. Balents, and M. P. A. Fisher, Phys. Rev. Lett. **76**, 2782 (1996)